Journal of the Korean Physical Society, Vol. 66, No. 9, May 2015, pp. 1422∼1425

Synthesis of Highly Crystalline Ga-doped Zinc-oxide Nanoparticles for Hybrid Polymer Solar Cells

Hye-Jeong Park, Kang Hyuck Lee and Ivaturi Sameera
School of Advanced Materials Science and Engineering, Sungkyunkwan University (SKKU), Suwon 440-746, Korea

Sang-Woo Kim*
School of Advanced Materials Science and Engineering, Sungkyunkwan University (SKKU), Suwon 440-746, Korea and SKKU Advanced Institute of Nanotechnology (SAINT) and Center for Human Interface Nanotechnology (HINT), SKKU, Suwon 440-746, Korea

(Received 3 November 2014, in final form 31 December 2014)

Gallium (Ga)-doped zinc-oxide (ZnO) nanoparticles (NPs) were synthesized by using a polymer pyrolysis method. The smallest size of the obtained 4-mol% Ga-doped zinc-oxide (GZO) spherical NPs was approximately 10-15 nm, and the presence of Ga was confirmed by using X-ray photoelectron spectroscopy. To examine the role of GZO NPs, fabricated hybrid polymer solar cells (HPSCs) by using blends of a conjugated polymer poly (3-hexalthiophene) as an electron donor and crystalline GZO NPs as an electron acceptor. Significant improvements in the short-circuit current density and fill factor compared to these for the undoped ZnO (UZO) NPs were achieved by using the GZO NPs. This suggests that the GZO NPs have higher electron mobility than the UZO NPs and possess great potential for use as electron acceptor in HPSCs.

PACS numbers: 61.72.Vv, 72.40.+w, 74.62.Bf
Keywords: Ga-doped ZnO nanoparticles, Hybrid polymer solar cells, Bulk heterojunction
DOI: 10.3938/jkps.66.1422

I. INTRODUCTION

Over the last few years, hybrid polymer solar cells (HPSCs) have attracted considerable attention due to their potential in low-cost manufacturing and low-temperature device processing, which allows these solution-based precursor materials to be deposited on flexible polymeric substrates and roll-to-roll fabrication to be used. HPSCs still have limited performance because of weak absorption in the visible long-wavelength region, low stability and poor charge transport. Therefore, improvements in the performance of the HPSCs have been actively explored through optimization of the materials, as well as the device structure. In recent years, a range of solution-processed bulk-heterojunction HPSCs using p-type conjugated polymers either in combination n-type polymers, fullerenes or with n-type inorganic semiconductor nanoparticles (NPs) has been reported. Typically, the inorganic NPs include PbS, CdS, CdTe, TiO_2, $CuInS_2$ and ZnO. Poly (3-hexythiophene) (P3HT) is commonly used as an electron donor in HPSCs. These hybrid polymer/inorganic NP solar cells are even advantageous in terms of the low-cost solution processing of the polymer semiconductor and the high electron mobility of the inorganic semiconductor NPs [1,2].

A great deal of scientific interest has been focused on identifying transparent conducting oxides for a wide range of devices. ZnO is one among such materials with good optical properties and a conductivity that increases with increasing oxygen-vacancy concentration. N-type doping of ZnO with X^{3+} metallic elements, such as aluminum (Al), gallium (Ga) and indium, induces considerable changes in its optical and electrical properties. Undoped ZnO (UZO) normally shows relatively high resistivity because of the low carrier concentration. Al has been used as the dopant in most studies on ZnO, but it has very high reactivity, leading to oxidation during nanoparticles growth, which reduces the expected improvements in the properties of the Al-doped ZnO NPs. However, Ga is less reactive and even resistant to oxidation than Al, which enhances the potential of using Ga-doped ZnO (GZO) NPs for desired applications. In addition, the covalent bond lengths of Ga−O and Zn−O are 1.92 Å and 1.97 Å, respectively. The slightly smaller bond length of Ga−O compared to Zn−O is an advan-

*E-mail: kimsw1@skku.edu; Fax: +82-31-290-7352

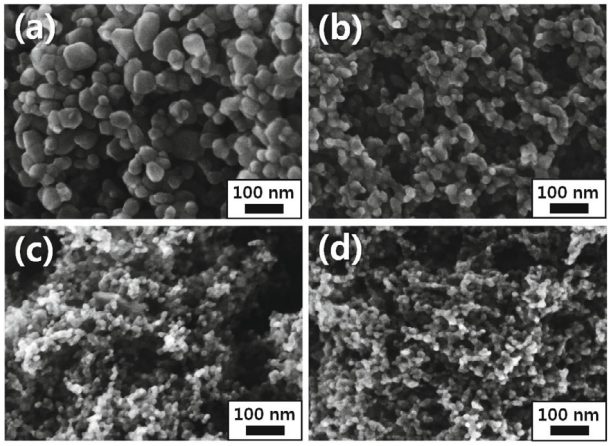

Fig. 1. FE-SEM images of GZO NPs derived from different concentrations of Ga dopant: (a) 0-mol%, (b) 2-mol%, (c) 4-mol%, and (d) 6-mol%.

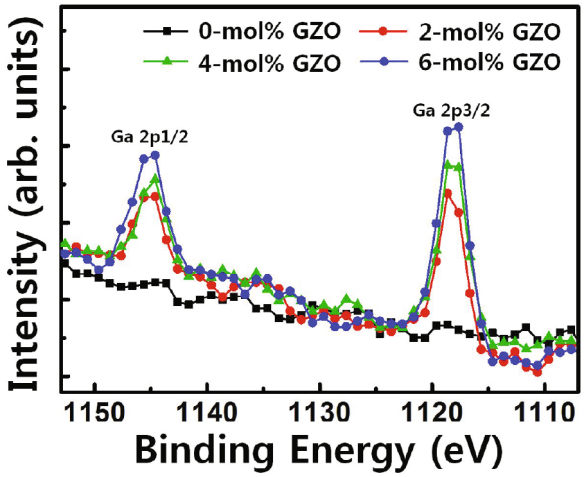

Fig. 2. (Color online) XPS spectra of Ga 2p peaks of ZnO NPs with different Ga contents (0-, 2-, 4- and 6-mol%).

tage because it can minimize the deformation of the ZnO lattice, even in the case of high gallium doping [3–5]. Owing to these advantages, many groups have reported the synthesis of GZO NPs by using several methods, which include chemical vapor deposition [6], the hydrothermal method [6], the sol−gel method [7], and evaporation [8]. Most of these techniques have some drawbacks, such as the requirement for large quantities of solution and organic materials, unsuitability for large-scale production, crystalline defects and wide particle-size distribution. Recently, the polymer pyrolysis method was developed. Therefore, this study focuses on the synthesis of high-quality crystalline GZO NPs, which can replace (6,6)-phenyl C_{61} butyric acid methyl ester (PCBM), and the experimental investigation of their suitability for use as electron acceptors in HPSCs.

II. EXPERIMENTS AND DISCUSSION

To prepare the GZO NPs via the polymer pyrolysis method, we dissolved zinc acetate in an aqueous acrylic acid solution (acrylic acid:H_2O = 70:30 wt.%) with stirring and heating at 80 °C. The advantages associated with polymer pyrolysis are the ease of operation, the use of a versatile range of metals, and the preparation of Ga-doped n-type semiconductors [9,10]. Doping was achieved by adding an appropriate amount of gallium nitrate hydrate into the solution at ratios of 0-, 2-, 4- and 6-mol%. To promote polymerization, we added 1 g of 5-wt.% ammonium persulfate aqueous solution as an initiator to an acrylic acid solution at 90 °C, and the mixed solution reacted to form a polyacrylate salt. The obtained final product was dried at 250 °C for 2 h, calcined at 600 °C for 4 h, and cooled naturally to room temperature. Using the as-prepared GZO NPs, blends of P3HT and GZO NPs in chlorobenzene were prepared by adding a 5-vol.% methanol solution with constant stirring at 60 °C. The solution was filtered through a microfilter with a pore size of 0.5 μm. For the fabrication of the HPSCs, blends of P3HT:GZO NPs (1:1 wt.%) was spin-coated at 1000 rpm onto ZnO thin films that had been deposited by using a sol-gel method. Thermal annealing at 150 °C for 10 min was then carried out. Subsequently, molybdenum oxide as an electron blocking layer and a silver anode were deposited by using thermal evaporation.

The structural investigation was performed using high-resolution transmission electron microscopy (HR-TEM, JEM-3010), and X-ray diffraction (XRD). Field-emission scanning electron microscopy (FE-SEM) was used to examine the NP's size. X-ray photoelectron spectroscopy (XPS) was used to confirm the presence of Ga. The HPSCs were characterized by using current density-voltage (J-V) measurements made with a solar simulator under AM 1.5G (100 mW/cm^2).

The FE-SEM images in Fig. 1 show the typical morphologies of the GZO NPs for Ga-doping concentrations of (a) 0-mol%, (b) 2-mol%, (c) 4-mol%, and (d) 6-mol%. The measured crystallite sizes of the UZO and the GZO NPs were approximately 20 ∼ 50 and 10 ∼ 25 nm, respectively. The presence of Ga profoundly influenced the formation of the NPs and their shapes and sizes.

The chemical bonding of the Ga dopant in the ZnO NPs was examined by using XPS, and the results are shown in Fig. 2. The two peaks, 1117.6 eV and 1144.6 eV, were assigned to the 2p3/2 and the 2p1/2 electronic states of atomic Ga, respectively. An energy gap of ∼27 eV is observed, which is also consistent with the value for element of Ga. For GZO NPs, a broad peak assigned to the 2p3/2 electronic state of Ga was clearly observed whereas in the UZO NPs, no peak related to Ga was detected. The explicit emergence of the Ga-related peak in the GZO sample suggests that Ga atoms were doped successfully into the ZnO lattices [11,12].

Figure 3 shows XRD patterns of the GZO NPs for

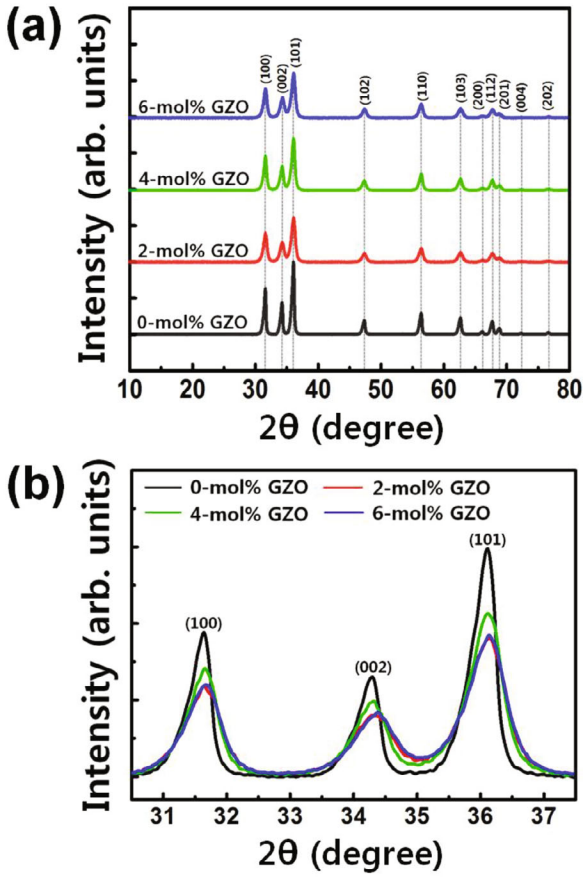

Fig. 3. (Color online) XRD patterns of UZO and GZO NPs with various concentrations: (a) overview of the XRD patterns and (b) expansion of the three main peaks.

Ga doping concentrations of 0-, 2-, 4- and 6-mol%. The XRD patterns of GZO NPs matched the diffraction pattern of hexagonal wurtzite ZnO. This indicates that the ZnO:Ga NPs have a polycrystalline hexagonal wurtzite structure. No additional peaks related to Ga or Ga_2O_3 were detected, indicating the high phase purity of the material. The broadening of the diffraction peaks from the samples was attributed to a decrease in crystallite size, which was calculated using Scherrer's formula: $G = 0.9\lambda/B\cos\theta_B$, where λ is the X-ray wavelength (1.5418 Å), θ_B is the maximum Bragg diffraction peak and B is the line width at half maximum [13]. The calculated crystallite sizes of GZO NPs with 0-, 2-, 4- and 6-mol% Ga doping were 20, 15, 12 and 11 nm, respectively. This indicates that introduction of Ga doping in ZnO changes the NP's morphology and decreases the primary NP size, which is consistent with the FE-SEM results. From the Ga-doped samples, slight shifts in the positions of the first three peaks were observed from Fig. 3(b). These shifts were attributed to the Ga dopants causing lattice disordering due to stress. In addition to the stress, the grains grew more easily when Ga was incorporated with ZnO. These peak shifts appeared to be caused by changes

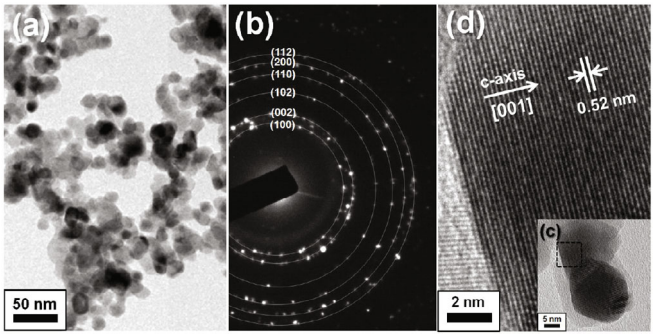

Fig. 4. Top-view HR-TEM images of the Ga 2-mol%-doped ZnO NPs: (a) low-resolution image, (b) selected area electron diffraction (SAED) and (c, d) high resolution images.

in the lattice parameters. Variations in the lattice parameters and, hence, the lattice volume are understood to arise because of two competing factors. The first factor is the size difference between the ionic radii of Zn^{2+} (0.74 Å) and Ga^{3+} (0.62 Å), and the second factor is deformation of the conduction band potential caused by an increase in the number of free carriers. As Ga is doped into ZnO, electrons are introduced into the system because of the dominant 3+ ionic nature of Ga ions and need remain confined inside the nanocrystals [14,15].

Figure 4 shows TEM images and selected area electron diffraction (SAED) of 2-mol% GZO NPs. Based on the low-magnification TEM image, the average size of the isolated GZO NPs was estimated to be 12 nm (Fig. 4(a)). The six rings observed in the SAED image (Fig. 4(b)) match with these for hexagonal ZnO crystals. A lattice spacing of 0.52 nm between adjacent lattice planes of a dispersed GZO NPs was calculated from the enlarged HR-TEM images of Fig. 4(c) and (d), and confirmed that the preferred growth direction of the GZO NPs was the [001] direction. The anisotropic growth of the GZO NPs along the [001] direction was due to the inherent polar properties of ZnO along the *c*-axis. For the GZO NPs, lattice fringes were clearly observed in the HR-TEM image, indicating high crystallinity without any grain boundaries.

Figure 5 shows the J-V characteristic curves of the solar cells fabricated using undoped and Ga-doped 2-, 4-mol% ZnO NPs. The HPSCs using 2-mol% GZO NPs had the best photovoltaic performance. The short-circuit current density (J_{sc}) and the fill factor (FF) of HPSCs using 2-mol% GZO NPs were improved by approximately 10% and 38% compared to these for UZO NPs. The improved performance can be attributed to the following reasons. First, the increase in the current density in the case of the HPSCs using GZO NPs may be increased carrier concentration due to Ga doping. However, the HPSCs with ZnO NPs having excessive Ga doping exhibit the opposite effect because of the excessive Ga region created by the solubility limit of Ga in ZnO effects as an impurity, which raises its resistivity [15–18]. Second, the

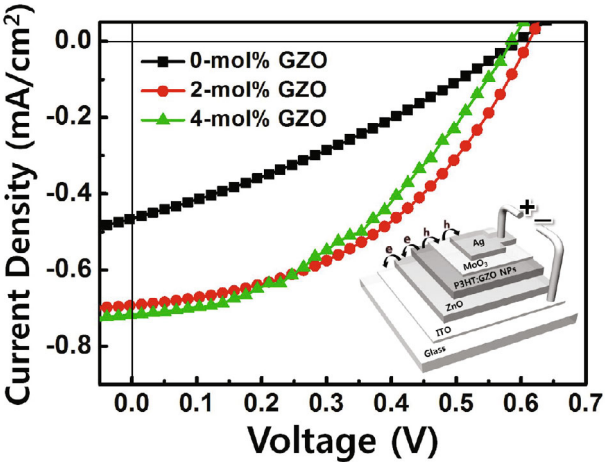

Fig. 5. (Color online) J-V characteristics of UZO NPs and GZO (2-, 4-mol%) NPs under AM 1.5 G simulated solar irradiation.

contact area with P3HT may increase due to the reduced size of GZO NPs, depending on the increased dopant amount. The morphology of the GZO NPs in the mixed active layer is very important as an efficient electron collection relies on continuous pathways for carriers. These facts lead to the overall improved photovoltaic properties, such as J_{sc} and FF, in the HPSCs with GZO NPs [19–23].

An improvement can be anticipated if an optimized condition of the morphology of the photoactive blend using GZO NPs can be achieved. Controling over the morphology of the blend by the proper choice of processing conditions is generally essential to reach this level of performance, and one of the traditional challenges in the field of bulk-heterojunction HPSCs lies in the optimization of the morphology.

III. CONCLUSION

In conclusion, UZO and GZO NPs were prepared by using a polymer pyrolysis method. Morphological and structural investigations using electron microscopy and X-ray diffraction confirmed the formation of smaller GZO NPs with high crystallinty compared to UZO NPs. X-ray photoelectron spectroscopy confirmed the doping of Ga atoms in the ZnO nanoparticles. Significant improvements of the short-circuit current density (J_{sc}) and the fill factor (FF) in HPSCs using GZO NPs rather than UZO NPs were observed, which suggests that GZO NPs have a higher electron mobility than UZO NPs.

ACKNOWLEDGMENTS

This study is supported by the Basic Science Research Program through the National Research Foundation of Korea (NRF) funded by the Ministry of Education, Science and Technology (2009-0083540) and by the Energy International Collaboration Research & Development Program of the Korea Institute of Energy Technology Evaluation and Planning (KETEP) funded by the Ministry of Knowledge Economy (MKE) (2011-8520010050).

REFERENCES

[1] W. J. E. Beek, M. M. Wienk and R. A. J. Janssen, Adv. Funct. Mater. **16**, 1112 (2006).
[2] P. A. C. Quist, W. J. E. Beek, M. M. Wienk, R. A. J. Janssen, T. J. Savenije and L. D. A. Siebbeles, J. Phys. Chem. **110**, 10315 (2006).
[3] C. Bundesmann, N. Ashkenov, M. Schubert, D. Spemann, T. Butz, E. M. Kaidashev, M. Lorenz and M. Grundmann, Appl. Phys. Lett. **83**, 1974 (2003).
[4] H. J. Ko, Y. F. Chen, S. K. Hong, H. Wenisch, T. Yao and D. C. Look, Appl. Phys. Lett. **77**, 3761 (2000).
[5] Z. F. Liu, F. K. Shan, Y. X. Li, B. C. Shin and Y. S. Yu, J. Cryst. Growth **259**, 130 (2003).
[6] S. Hartner, M. Ali, C. Schulz, M. Winterer and H. Wiggers, Nanotechnology **20**, 445701 (2009).
[7] S. Gong, Z. H. Chen, F. L. Tang, P. H. Pi, X. F. Wen, D. F. Zheng, J. Cheng and Z. R. Yang, J. Chin. Ceram. Soc. **37**, 648 (2009).
[8] F. F. Bai, Y. He, P. He, Y. W. Tang and Z. J. Jia, Mater. Lett. **60**, 3126 (2006).
[9] H. Sankur and J. T. Cheung, J. Vac. Sci. Technol. A **1**, 1806 (1983).
[10] T. Oku, K. Niihara and K. Suganuma, J. Mater. Chem. **8**, 1323 (1998).
[11] Z. Z. Ye, Y. J. Zeng, Y. F. Lu, S. S. Lin, L. Sun, L. P. Zhu and B. H. Zhao, Appl. Phys. Lett. **91**, 112110 (2007).
[12] K-S. Shin, H-J. Park, G. C. Yoon, S-W. Jeong, B. Kumar and S-W. Kim, J. Phys. Chem. C **117**, 24692 (2013).
[13] Z. B. Ayadi, L. E. Mir, K. Djessas and S. Alaya, Nanotechnology **18**, 445702 (2007).
[14] C. X. Xu, X. W. Sun and B. J. Chen, Appl. Phys. Lett. **84**, 1540 (2004).
[15] S. Cimitan, S. Albonetti, L. Forni, F. Peri and D. Lazzari, J. Colloid Inter. Sc. **329**, 73 (2009).
[16] H. Serier, A. Demourgues and M. Gaudon, Inorg. Chem. **49**, 6853 (2010).
[17] W. Korner and C. Elsasser, Phys. Rev. B **81**, 085324 (2010).
[18] S. V. Bhat, A. Govindaraj and C. N. R. Rao, Sol. Energ. Mat. Sol. Cells **95**, 2318 (2011).
[19] Y. Zhou, M. Eck and M. Kruger, Energy Environ. Sci. **3**, 1851 (2010).
[20] J. Zhong, S. Muthukumar, Y. Chen and Y. Lu, Appl. Phys. Lett. **83**, 3401 (2013).
[21] S. D. Oosterhout, M. M. Wienk, S. S. Bavel, R. Thiedmann, L. J. A. Koster, J. Gilot, J. Loos, V. Schmidt and R. A. J. Janssen, Nat. Mater. **8**, 818 (2010).
[22] R. Wang and A. W. Sleight, Chem. Mater. **8**, 433 (1996).
[23] S-S. Li, C-P. Chang, C-C. Lin, Y-Y. Lin, C-H. Chang, J-R. Yang, M-W. Chu and C-W. Che, J. Am. Chem. Soc. **133**, 11614 (2011).